Author/s:
Holmes, D;Wilhelm, B;Jakob, AM;Yu, X;Hudson, FE;Itoh, KM;Dzurak, AS;Jamieson, DN;Morello, A

Title:
Improved Placement Precision of Donor Spin Qubits in Silicon using Molecule Ion Implantation

Date:
2024-03

Citation:
Holmes, D., Wilhelm, B., Jakob, A. M., Yu, X., Hudson, F. E., Itoh, K. M., Dzurak, A. S., Jamieson, D. N. & Morello, A. (2024). Improved Placement Precision of Donor Spin Qubits in Silicon using Molecule Ion Implantation. Advanced Quantum Technologies, 7 (3), https://doi.org/10.1002/qute.202300316.

Persistent Link:
https://hdl.handle.net/11343/345443

ADVANCED QUANTUM TECHNOLOGIES
www.advquantumtech.com

Improved Placement Precision of Donor Spin Qubits in Silicon using Molecule Ion Implantation

Danielle Holmes, Benjamin Wilhelm, Alexander M. Jakob, Xi Yu, Fay E. Hudson, Kohei M. Itoh, Andrew S. Dzurak, David N. Jamieson, and Andrea Morello*

Donor spins in silicon-28 are among the best performing qubits in the solid state, offering unmatched coherence times, gate fidelities beyond 99% and the ability to fabricate arrays using deterministic ion implantation. Donor placement precision is improved upon, advantageous for qubit readout and coupling, by implanting molecule ions that carry bystander atoms to boost the detection confidence. Here, the suitability of phosphorus difluoride (PF_2) molecule ions is demonstrated to fabricate ^{31}P donor qubits. Using secondary ion mass spectrometry, it is confirmed that ^{19}F (nuclear spin $I = 1/2$) diffuses away from the implant site while ^{31}P remains close to its original location during a donor activation anneal. Electron spin resonance measurements are then performed on PF_2-implanted qubit devices. A pure dephasing time of $T_2^* = 20.5 \pm 0.5\,\mu s$ and a coherence time of $T_2^{Hahn} = 424 \pm 5\,\mu s$ are extracted for the P donor electron- values comparable to those found in conventional atomic ^{31}P-implanted qubit devices. Additionally, the P donor electron is not found to hyperfine couple to any ^{19}F nuclear spins in its vicinity. Molecule ions therefore show great promise for producing high-precision deterministically-implanted arrays of long-lived donor spin qubits.

1. Introduction

Semiconductor spin qubits[1,2] are appealing platforms for the construction of scalable quantum computers. On the classical engineering side, they offer compatibility with standard semiconductor microelectronics manufacturing processes; on the quantum side they have recently crossed the threshold of one- and two-qubit logic gate fidelities exceeding 99%.[3–6] Among the possible physical qubit implementations in semiconductors, donor (also referred to as 'dopant' or 'impurity') atoms in silicon were the first to be proposed[7] and experimentally demonstrated[8,9] as spin qubits. With the introduction of an isotopically enriched ^{28}Si host matrix, which possesses a significantly reduced residual ^{29}Si content (< 0.1%[10]), donor spin qubits have achieved extraordinary values of spin coherence times, both in bulk[11,12] and in single-atom nanoscale devices.[13] As eloquently stated in a recent review,[14] 'Impurity spins hold record coherence times in each category where data for them exist'.

The key challenge for donor spin qubits is the development of fabrication methods to place and control individual atoms with sufficient precision, within scalable nanoelectronic structures. There exist two different ways to do so. One involves the use of scanning tunneling microscope (STM) lithography[15,16] to define a hydrogen mask through which phosphine (PH_3) molecules are absorbed onto Si, and the P atoms are subsequently incorporated in the crystal. This method yields sub-nanometre placement precision, and a very clean crystalline environment for the spins,[17] but typically results in multiple P atoms incorporated in tightly-spaced clusters.[18] The other, adapted from the classical semiconductor industry,[19] involves the implantation of individual dopant atoms into the crystal.[20,21] This method retains compatibility with the standard metal-oxide-semiconductor (MOS) fabrication workflow, and has been developed to deterministically implant single ^{31}P dopants sub-25 nm deep with ≈ 99.9% detection confidence.[22] All demonstrations of coherent single-atom spin control to date have been achieved with ion-implanted donors.[23] However, ion straggling typically causes >10 nm uncertainty in the final placement position of ^{31}P, which calls for creative ways to design two-qubit logic gates that are insensitive to such uncertainty.[24–26] In this work, we demonstrate a technique

D. Holmes, B. Wilhelm, X. Yu, F. E. Hudson, A. S. Dzurak, A. Morello
Centre for Quantum Computing and Communication Technology
School of Electrical Engineering and Telecommunications
University of New South Wales
Sydney, NSW 2052, Australia
E-mail: danni.holmes@unsw.edu.au

A. M. Jakob, D. N. Jamieson
Centre for Quantum Computing and Communication Technology
School of Physics
The University of Melbourne
Melbourne, VIC 3010, Australia

F. E. Hudson, A. S. Dzurak
Diraq
Sydney, NSW 2052, Australia

K. M. Itoh
School of Fundamental Science and Technology
Keio University
3-14-1 Hiyoshi, Kohoku-ku, Yokohama 223-8522, Japan

The ORCID identification number(s) for the author(s) of this article can be found under https://doi.org/10.1002/qute.202300316

DOI: 10.1002/qute.202300316

that reduces the straggle-related dopant placement uncertainty upon implantation without compromising on the single ion detection confidence. The presented approach enables donors to be located closer to the gate oxide interface with an increased tunnel coupling to the single electron transistor (SET), resulting in a faster qubit readout and initialization.

In order to produce ultra-scaled arrays of implanted donor spin qubits required for quantum error correction architectures in fault-tolerant quantum computers, a high single ion detection confidence is essential to ensure the accurate counting of donor ions into the Si substrate. This requirement poses a formidable challenge, since a low ion implantation energy ($\approx 8-20$ keV) is required to place donor qubits in close proximity to the gate oxide interface ($\approx 7-20$ nm) for reliable spin readout via tunneling to an SET and electrostatic tuning by surface nanoelectronics.[22,27] Low ion implantation energies generally reduce the detection signal, which consists of the charge induced by the generation of electron-hole pairs by the electronic stopping processes of the ion as it slows down in the Si substrate. The detection confidence of a single implanted ion is determined by the signal-to-noise ratio of this ion beam induced charge (IBIC) signal pulse. Recent advances in single ion detector design, materials quality and low-noise electronics have led to the demonstration of detection fidelities up to 99.85% for single implanted P donors at an energy of 14 keV.[22] However, the placement of donors closer to the surface and the reduction of straggle requires an even lower implant energy.

Here, we demonstrate the use of molecule ions as a way to retain large implantation energies, and thus IBIC signals, while reducing the implantation depth and straggle of the donor qubit. Molecule ions are commonly used in the microelectronics industry for the formation of ultra-shallow junctions, crucial in the fabrication of MOS field-effect transistors with decreasing device dimensions for increased component density. For example, boron difluoride (BF_2) molecule ions are favored over atomic boron (B) ions to produce shallow implanted p-type regions in Si due to their smaller projected range, their ability to induce amorphization of Si to suppress ion channeling[28] and to eliminate damage during solid-phase epitaxial regrowth[29,30] and the ability of the co-implanted F to reduce boron transient enhanced diffusion.[31]

In this work, we employ phosphorus difluoride (PF_2^+) molecule ions to fabricate P donor qubits, shown schematically in **Figure 1**. The P donor carries a fraction of the molecule ion's energy in proportion to its mass. Upon impact, the molecule ion breaks apart since the implant energy is much larger than the molecular binding energy, effectively co-implanting separate atomic ions at the same exact impact site. P donors can be placed to a depth of ≈ 15 nm below an 8 nm gate oxide, suitable for spin initialization and readout, by implanting PF_2^+ molecule ions at an energy of 19.5 keV. Under these conditions, the P donor carries an energy of ≈ 9 keV, resulting in a low straggle of < 8 nm. The F bystander ions within the molecule ion carry the remaining energy, and have been shown to boost the IBIC signal further above the noise threshold of the detector.[32]

Fluorine nuclei have a spin ($I = 1/2$) and a large gyromagnetic ratio. Spin fluctuations of ^{19}F nuclei close to the P donor qubit (i.e. at distances of order the Bohr radius, 1.8 nm for P in Si[33]) would cause perturbations in the local magnetic field at the donor site, resulting in a time-varying qubit resonance frequency

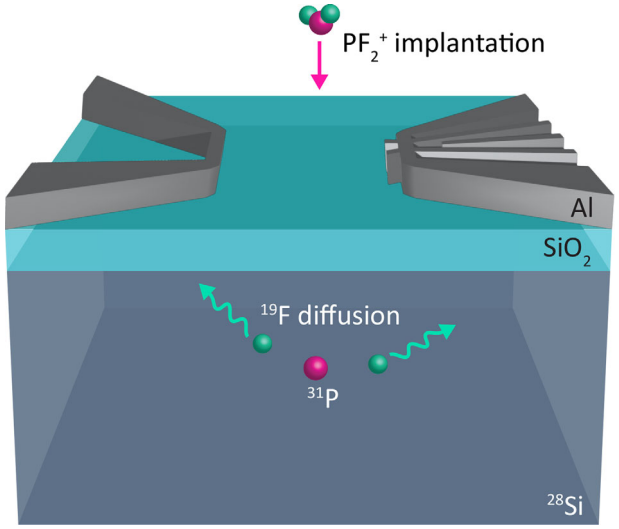

Figure 1. A donor spin qubit device fabricated using the implantation of PF_2^+ molecule ions. The bystander ^{19}F ions diffuse away from the active region of the device upon a donor activation anneal, while the ^{31}P donor qubit remains close to the original stopping location.

and consequent reduction of the electron spin coherence time.[34] Fortunately, F is known to be an ultra-fast diffuser in Si.[35] We show that F diffuses away from the active region of qubit devices while the P donors remain close to their original location during a donor activation anneal, using secondary ion mass spectrometry (SIMS).

For the first time, we demonstrate the operation of a donor qubit produced using the implantation of a molecule ion. The suitability of PF_2 for making long-lived P donor qubits was confirmed by fabricating PF_2-implanted qubit devices and performing electron spin resonance (ESR) measurements. The P donor electron was not found to couple to any ^{19}F nuclear spins.

2. Experimental Section

Intrinsic crystalline Si substrates were implanted with PF_2^+ molecule ions with various implantation energies and fluences using a Colutron ion implanter with a gas source consisting of 5% PF_5 diluted in 95% Ar, as summarised in **Table 1**. Samples were implanted at room temperature, with a beam line pressure of $\approx 5 \times 10^{-8}$ Torr and a substrate tilt of 7° relative to the incident beam axis to suppress ion channeling.

Table 1. Implant parameters for the samples measured in this work.

	Sample A	Sample B	Sample C
Implant species	PF_2^+	PF_2^+	PF_2^+
Implant energy (keV)	20	20	19.5
Implant fluence (cm^{-2})	3×10^{14}	3×10^{14}	2×10^{11}
Anneal (°C, s, ambient)	None	1050, 5, Ar	1000, 5, N_2
Measurement	SIMS	SIMS	ESR

To determine the diffusion of P and F in Si due to a rapid thermal anneal (RTA), samples A and B were measured using SIMS. To produce samples A and B, intrinsic natural < 100 > Si substrates with a native oxide surface layer were implanted with 20 keV PF_2^+ ions at a fluence of 3×10^{14} cm^{-2}. This implantation results in a peak concentration of P and F of 1.5×10^{20} cm^{-3} and 3×10^{20} cm^{-3}, respectively, at a depth of ≈ 15 nm below the surface. The implant fluence was chosen to ensure the P and F concentrations are well above the minimum detectable limit for SIMS analysis and is around three orders of magnitude higher than those employed for qubit fabrication. Sample A was left as-implanted, while sample B was annealed at 1050 °C for 5 s in an argon atmosphere. Due to the shallow implant profile, both samples were capped with a 50 nm Pt layer to increase the accuracy of the SIMS analysis near the Si surface. The details of the SIMS measurement is provided in the following.

To determine the suitability of PF_2 molecule ions for producing long-lived P donor qubits, sample C had a nanoelectronic qubit device fabricated on-chip to perform ESR of the P donor qubit. To produce sample C, a ^{28}Si epilayer with a high quality 8 nm gate oxide was implanted with 19.5 keV PF_2^+ ions at a fluence of 2×10^{11} cm^{-2} through a 100 μm diameter aperture into a 90 nm × 100 nm implant window. This implantation results in a peak concentration of P and F of ≈ 1.1×10^{17} cm^{-3} and ≈ 1.9×10^{17} cm^{-3} and an average implanted depth of ≈ 8 and ≈ 7 nm below the Si/SiO_2 interface, respectively. This sample was then given an RTA at 1000 °C for 5 s in a nitrogen atmosphere. Surface nanoelectronics were then fabricated as standard for our qubit devices using multiple layers of electron beam lithography and aluminium deposition. This device was then packaged and cooled to around 19 mK in a dilution refrigerator. Details of the ESR measurements are provided in the following.

3. Minimizing Qubit Placement Uncertainty

In supporting work, we found that 9 keV P^+ ions implanted into on-chip single ion detectors resulted in a detection confidence of ≈ 98.6%.[32] This implantation energy can be simulated using the Stopping and Range of Ions in Matter (SRIM) Monte-Carlo model[36] to have an average range of ≈ 16 nm below the sample surface and a longitudinal straggle of ≈ 8 nm. If we instead utilize PF_2^+ ions, implanted at an energy of 19.5 keV to maintain the fraction of energy carried by P to be ≈ 9 keV, we could boost the detection confidence to over 99.95%. This result clearly shows the ability of the bystander F ions to shift the IBIC signal further above the noise floor of the detector without increasing the average implanted range or straggle of the P donor.

Without the use of molecule ions, to achieve a detection confidence of ≈ 99.95%, we would require a P implantation energy of ≈ 15 keV. This increased energy would result in an increased average implanted range of ≈ 24 nm and an increased longitudinal straggle of ≈ 11.5 nm, with a distribution shown in **Figure 2**a simulated by implanting 200,000 P ions in Si at an energy of 15 keV using SRIM. The corresponding simulated P distribution that results from the implantation of 19.5 keV PF_2 molecule ions, approximated by implanting 200,000 8.757 keV P ions, is shown in Figure 2b. In addition, Crystal-TRIM simulations[22,37] were performed to account for ion channeling down crystallographic axes

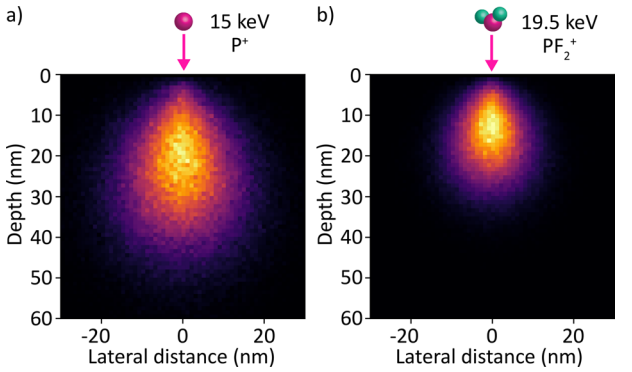

Figure 2. SRIM simulation of the P ion distribution resulting from the implantation of a) 15 keV P^+ ions and b) 19.5 keV PF_2^+ ions into Si. The color scale represents the probability distribution of the P donors. Effects from ion channelling were neglected.

of Si. These show that 35.5% (11.6%) of 15 keV (8.757 keV) P ions that are transmitted through an 8 nm SiO_2 layer end up deeper than 20 nm below the oxide interface, out of the readout range for a surface SET. These simulations showcase the ability of PF_2 molecule ions to minimize the donor qubit implantation depth and placement uncertainty without compromising on the single ion detection confidence.

The reduced donor placement uncertainty has positive implications on the scalability of deterministically implanted arrays of donor spin qubits in Si. For the case of flip-flop qubits, the lateral placement precision is unimportant, since the electric dipole mediated coupling has a strength that can be held constant over a wide range of inter-donor separations (≈ 180 − 500 nm) by electrically tuning the electron wavefunctions involved.[26] However, the vertical placement precision is key to their operation, since it determines the electron tunnel coupling between the donor and the interface potential wells. This will be substantially improved by PF_2 molecule implants. For electron spin qubits, we have recently demonstrated entangling two-qubit logic gates based on the exchange interaction,[38] using a method that does not require atomic precision in the relative donor placement,[24] as long as the exchange coupling is smaller than the hyperfine interaction (≈ 100 MHz) and larger than the electron spin resonance linewidth (≈ 10 kHz). Improving the placement precision by using PF_2 molecule implants will further increase the yield of donor pairs located within the useful range for the exchange interaction.[39]

4. Fast Diffusion of Fluorine

As standard practice after the implantation of P donor qubits, samples are given a rapid thermal anneal at 1000 °C for 5 s in a nitrogen atmosphere. This is to repair the damage to the Si crystal caused by ion implantation and to ensure that the P donor is substitutional in the Si lattice and electrically active.[40,41] The diffusion of both P and F dopants in Si as a result of this rapid thermal anneal was determined by measuring the concentration depth profiles with SIMS, before and after annealing.

Samples A and B were analyzed with time-of-flight secondary ion mass spectrometry (TOF-SIMS) in negative polarity by Bi^+

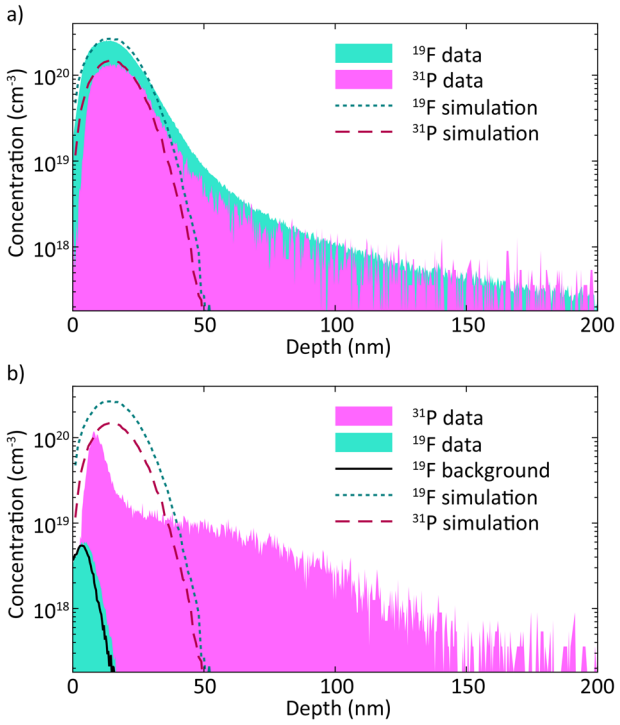

Figure 3. SIMS measurements show the concentration of P and F as a function of depth below the Si surface for a) sample A and b) sample B. The colored dashed lines show the depth profiles of P and F simulated using SRIM for an implantation of 20 keV PF_2 at a fluence of 3×10^{14} cm^{-2}. The black dashed line in b) shows the background F concentration present in sample B outside of the implanted region.

ions at 30 keV, sputtered by Cs^+ ions at 500 eV. The concentration of both P and F as a function of depth below the Si surface, before and after the RTA required for donor activation, is given in **Figure 3**.

The implantation profiles of both F and P before the RTA are given in Figure 3a. The measured concentration profiles are in good agreement with the simulated profiles produced using SRIM (dashed lines) in the near-surface region up to a depth of ≈ 30 nm. The simulated concentration of F and P is lower than measured at greater depths due to the SRIM simulation not taking into account ion channelling into the crystalline Si target.

The P depth profile, measured by SIMS and shown in Figure 3b, shows two noticeable features that appear after the RTA. First, a sharpened concentration peak at ≈ 9 nm below the Si surface resulted from an outdiffusion of P toward the surface. Second, a tail extended beyond ≈ 100 nm deep resulting from an indiffusion of P donors toward greater depths below the Si surface. The first feature is caused by transient enhanced diffusion (TED), whereby the elevated presence of self-interstitials, i.e., Si atoms occupying non-lattice sites, introduced to the crystal by damage caused by ion implantation enhances the diffusion of P.[42] In TED, a large interstitial gradient arises during annealing due to interstitial recombination at the oxide interface. This generates a large flux of interstitials toward the interface, driving P in the same direction through a kick-out mechanism.[43] For the second feature, the 'boxlike' nature of the indiffusion tail is characteristic of the chemical pumping of interstitials into the bulk during annealing by the high concentrations of P near surface, in turn enhancing P diffusion.[43] However, both diffusion mechanisms are greatly reduced in donor qubit devices. This is due to the donor implantation fluence being more than three orders of magnitude lower, resulting in a significantly reduced concentration of interstitials[44] and P donors,[43] respectively. The diffusion length of P in donor qubit devices during a donor activation anneal is closer to the intrinsic diffusion length of ≈ 2 − 3 nm[45] and thus lower than the spatial straggling upon ion implantation. In addition, the co-implantation of F has been shown to reduce TED of P in Si.[46] This SIMS measurement therefore demonstrates that the P diffusion during a standard RTA is as expected from literature. It is commensurate with P donors remaining close to their implanted locations in the active region of donor spin qubit devices when introduced using molecule ions.

On the contrary, Figure 3b shows that F atoms diffuse significantly away from their as-implanted profile during the RTA. In fact, the concentration of ^{19}F found in the active near-surface region of a donor qubit device after annealing is identical to the background ^{19}F level, measured in a region where no PF_2^+ ions were implanted (black dashed line in Figure 3b)). Hence, this measured ^{19}F profile exclusively results from ^{19}F contamination in the sputter-deposited Pt capping layer that is forward recoiled into the Si substrate during the SIMS measurement. Fluorine implanted at low energies and fluences has been shown to outdiffuse to the Si surface where it outgasses, reducing the amount of F present in the sample.[35] Implanted F is known to diffuse rapidly at temperatures above 550 °C, where substitutional F is thought to dissociate into interstitial F and a vacancy.[47] The liberated interstitial F subsequently undergoes ultra-fast diffusion through Si with an activation energy of only ≈ 0.7 eV,[48] distributing F throughout the entire Si sample at concentrations well below the SIMS detection limit in seconds. In qubit devices with a high quality gate oxide, a fraction of the implanted F may be gettered at the Si/SiO_2 interface during annealing. F has been shown to passivate dangling bonds at the interface through the formation of Si-O-F and Si-F complexes, which would have the beneficial effect of reducing noise in qubit devices.[49]

The SIMS data shows that after the RTA required to activate the implanted P donors, there is no additional concentration of F in the active region of qubit devices due to the implantation of PF_2^+ molecule ions. This result shows PF_2 molecule ions to be a promising alternative to introducing long-lived P donor qubits into Si devices via implantation as they should not contribute any significant levels of spin-containing nuclei to the qubit environment.

5. ^{31}P Donor Spin Qubit Measurements

To determine the suitability of PF_2 molecule ions for producing high quality implanted ^{31}P donor spin qubits, a nanoelectronic qubit device[3] was fabricated on the surface of sample C to operate one of the ^{31}P donors, introduced via PF_2 ion implantation, as an electron spin qubit.[8] Sample C was mounted on the mixing chamber of a dilution refrigerator, with a base temperature ≈ 19 mK and an electron temperature ≈ 150 mK. An external magnetic field with strength $B_0 \approx 1.4$ T was applied along the z-axis using a superconducting solenoid, resulting in a Zeeman

splitting of the electronic and nuclear spin states. The Hamiltonian of the donor system can then be written as[8,9]

$$H = \gamma_e B_0 \hat{S}_z - \gamma_n^P B_0 \hat{I}_z^P + \sum_k A^k \hat{\boldsymbol{S}}.\hat{\boldsymbol{I}}^k \quad (1)$$

where the donor electron and ^{31}P nuclear spins have gyromagnetic ratios $\gamma_e \approx 27.97$ GHz/T[50] and $\gamma_n^P \approx 17.23$ MHz/T,[51] respectively, and $\hat{S}_z$ and $\hat{I}_z^P$ are the electron and ^{31}P nuclear spin projection operators, respectively. The donor electron is hyperfine coupled to k nuclei residing within its Bohr radius, each with a coupling strength A^k and a nuclear spin $\hat{\boldsymbol{I}}^k$. This final term is often simplified to contain solely the hyperfine coupling between the donor electron and the ^{31}P nucleus, $A^P \hat{\boldsymbol{S}}.\hat{\boldsymbol{I}}^P$. The hyperfine couplings to other nearby nuclei, such as residual ^{29}Si, are orders of magnitude smaller[52] and their effect is usually handled as a source of decoherence.[34]

Nanoelectronic structures on the surface of the chip provide electrostatic control of the donors, create a single-electron transistor (SET) charge sensor, and deliver microwave and radio-frequency signals through a broadband antenna (Figure 1). With this set-up, we can perform single-shot electron spin readout,[53] and high fidelity (approximately 99.9%) single-shot quantum nondemolition readout of the nuclear spins,[9] as well as nuclear magnetic resonance (NMR) and ESR[8] on all spins involved.

The presence of a ^{31}P donor in our qubit device was first confirmed by acquiring an adiabatic ESR spectrum, as shown in **Figure 4a**. The spectrum was obtained by sweeping the centre frequency, f, of an applied microwave chirp signal designed to adiabatically invert the electron spin,[54] around $\gamma_e B_0 \approx 39$ GHz and measuring the probability of the electron being found in the spin up state. A high spin up proportion ('ESR peak') is measured when the frequency range covered by the adiabatic sweep encompasses the ESR frequency. The two observed ESR peaks are split by the hyperfine coupling to an $I = 1/2$ ^{31}P nuclear spin, with a strength of $A^P \approx 115$ MHz, which is close to the bulk value for P donors in Si of 117.5 MHz.[50] Random switches are observed between the two ESR peaks, corresponding to quantum jumps of the nuclear spin state.[9] No further splitting of ESR peaks due to hyperfine coupling to additional nuclei was observed on this scale since the adiabatic ESR spectrum shows a linewidth artificially broadened by the width of the frequency chirp, 3 MHz in this case.

In order to assess the quality of the PF_2-implanted donor spin qubit, the donor electron pure dephasing time, T_2^*, and coherence time, T_2^{Hahn}, were measured using Ramsey and Hahn echo pulse sequences, respectively.[8,13] The Ramsey experiment was performed using the pulse sequence given in the inset of Figure 4b. Fitting the data with a sinusoidal Gaussian decay yields an electron pure dephasing time of $T_2^* = 20.5 \pm 0.5\mu$s. The Hahn echo experiment was performed using the pulse sequence given in the inset of Figure 4c. Fitting the data with a sinusoidal Gaussian decay yields an electron coherence time of $T_2^{\text{Hahn}} = 424 \pm 5\mu$s. These values are comparable to previous donor qubit devices implanted with atomic P ions that have been measured in the same dilution refrigerator. While this result is promising, it does not in itself prove that co-implanted F bystander ions do not negatively impact the P donor qubit since the donor qubit coherence time can depend on the details of the specific device, dilution refrigerator, magnet, and measurement setup.

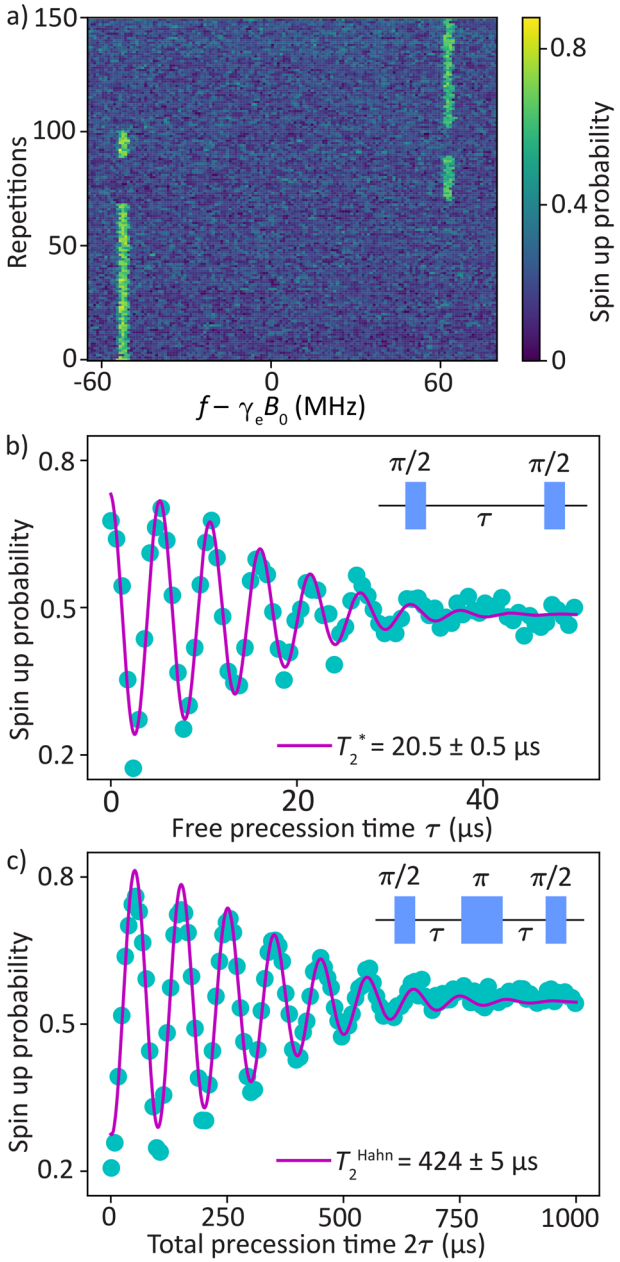

Figure 4. a) Adiabatic ESR spectrum of a ^{31}P donor electron in Si. Two ESR peaks are visible with a splitting of ≈ 115 MHz due to the hyperfine coupling to the $I = 1/2$ nuclear spin of the ^{31}P donor. b) Ramsey measurement on the ^{31}P donor electron with the corresponding pulse sequence shown in the top right. The fit yields a pure dephasing time $T_2^* = 20.5 \pm 0.5\mu$s. c) Hahn echo measurement on the ^{31}P donor electron with the corresponding pulse sequence shown in the top right. The fit yields a coherence time $T_2^{\text{Hahn}} = 424 \pm 5\mu$s.

The pulse sequence to detect weakly-coupled ^{29}Si or ^{19}F nuclei is given in **Figure 5a**. First, the ^{31}P donor nucleus is initialized in the spin down state to ensure that the frequency of the lower

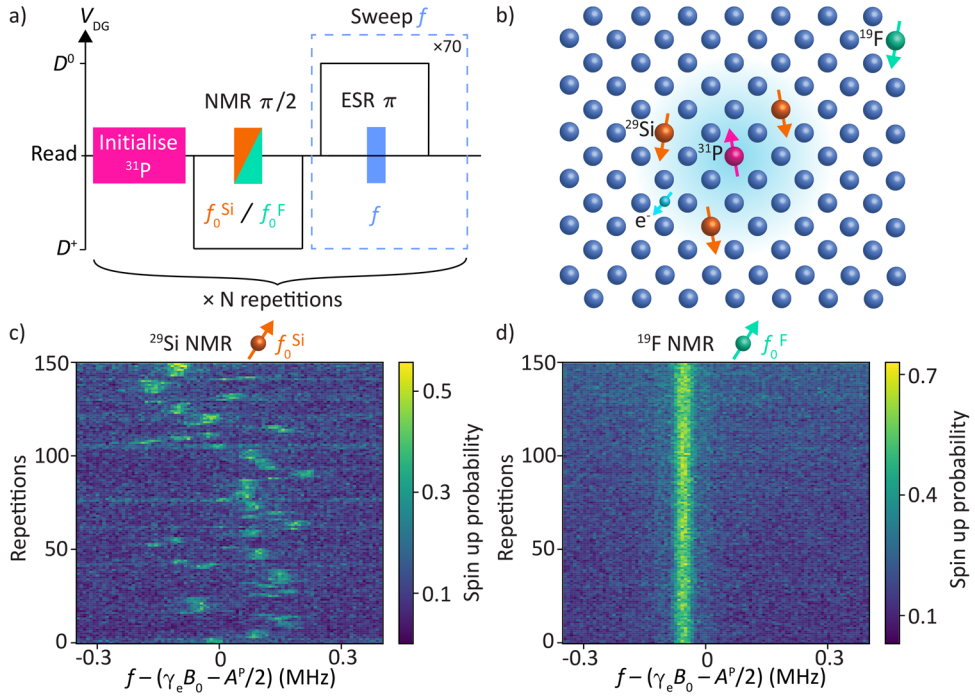

Figure 5. a) Pulse sequence used to flip the spins of ^{29}Si or ^{19}F nuclei while monitoring the P donor ESR spectrum. b) The Bohr radius of the P donor electron encompasses multiple ^{29}Si spins but no ^{19}F spins. c) Coherent ESR spectrum of the lower hyperfine split P donor ESR peak. The P donor electron spin up probability is measured as a function of ESR frequency for multiple repetitions, interleaved with ^{29}Si NMR $\pi/2$ pulses. The instantaneous ESR frequency is seen to jump frequently between discrete values, determined by the orientation of a few ^{29}Si nuclear spins, hyperfine coupled to the P electron with strengths of order 100 kHz. d) The same experiment repeated with NMR $\pi/2$ pulses applied at the expected resonance of ^{19}F nuclei, interleaved with the collection of coherent ESR spectra. The ESR frequency remains completely stable, indicating that no ^{19}F are coupled to the P donor electron.

hyperfine-split ESR peak can be tracked continuously. Next, the donor is prepared in the ionized state, D^+, by lowering the voltage on a donor gate, V_{DG}, to remove the donor electron. An NMR $\pi/2$ pulse is then applied on resonance with ^{29}Si or ^{19}F nuclei, with a frequency of $f_0^{Si} = \gamma_n^{Si} B_0$ or $f_0^F = \gamma_n^F B_0$, respectively, to flip approximately half of the coupled nuclei. The $\pi/2$ pulse duration for ^{29}Si and ^{19}F NMR was determined from the respective Rabi frequencies, Ω^k, calculated from the measured Rabi frequency of the ionized ^{31}P donor nucleus, Ω^P, scaled by the respective gyromagnetic ratios, $\Omega^k = (\gamma_n^k/\gamma_n^P)\Omega^P$. The donor is then brought into the neutral state, D^0, by raising V_{DG} to ensure that the donor electron remains bound to the ^{31}P nucleus. An ESR π pulse is then applied at a frequency f and the donor is brought to the read position with V_{DG}. This is repeated 70 times to measure the spin up probability of the donor electron. The ESR frequency is then swept around the lower hyperfine-split ESR peak at $f = \gamma_e B_0 - A^P/2$. The entire pulse sequence is then repeated N times to track the resonant frequency of the donor electron from the ESR spectra collected after each NMR $\pi/2$ pulse.

First, this measurement was performed using NMR pulses on resonance with ^{29}Si nuclei, with the data shown in Figure 5c. The ESR frequency of the P donor electron can be seen to jump between multiple values at short time intervals. The ^{29}Si NMR pulses that we apply are therefore changing the spin configuration of the ^{29}Si nuclei that are coupled to the P donor electron. This experiment confirms the presence of ^{29}Si nuclei within the Bohr radius of the P donor electron.

The measurement was then repeated using NMR pulses on resonance with ^{19}F nuclei, with the data shown in Figure 5d. The ESR frequency of the P donor electron can be seen to remain constant over 150 repetitions of the pulse sequence, corresponding to a time period of ≈ 20 min. The ^{19}F NMR pulses that we apply are therefore not changing the spin configuration of any nuclear spins that are coupled to the P donor electron. We note that it is quite normal, in the absence of active NMR stimuli at the ^{29}Si resonance frequency, for the ^{29}Si nuclei to remain unchanged over very long time scales, thanks to the phenomenon of 'nuclear freezing'.[55] This investigation leads to the positive result that no ^{19}F nuclear spins are coupled to the P donor electron spin qubit, to within the intrinsic ESR linewidth of our experiment. This observation confirms the expectation, already supported by the SIMS data (Figure 3), that the F bystander ions diffuse away from the active region of the qubit device upon performing a donor activation anneal.

6. Conclusion

In conclusion, we demonstrate that molecule ions can be employed to boost the placement precision and scalability of deterministic implantation of donor qubits without compromising on qubit quality. The F bystander ions that are co-implanted with the ^{31}P donor boost the detection confidence of implanted single ions by increasing the ion beam induced charge signal further above the detector noise floor. Using secondary ion

mass spectrometry, we find that ^{19}F diffuses away from the active region of qubit devices while the P donors remain close to their original location during a donor activation anneal. We then fabricated PF_2-implanted qubit devices and performed ESR measurements to determine that the P donor electron showed coherence times comparable to conventional ^{31}P donor qubits produced via atomic ^{31}P ion implantation. The ESR spectrum of the P donor electron was then monitored while applying NMR pulses on resonance with particular nuclear species to show that the P donor electron was not coupled to any nearby ^{19}F nuclear spins, only to residual ^{29}Si nuclei present in the isotopically enriched ^{28}Si epilayer. By improving the spatial donor placement precision and preserving the single ion detection confidence, deterministic single PF_2 molecule ion implantation constitutes a promising concept for the realization of scalable and long-lived ^{31}P donor qubit networks.

Acknowledgements

This research was funded by the Australian Research Council Centre of Excellence for Quantum Computation and Communication Technology (CE170100012) and the US Army Research Office (Contracts no. W911NF-17-1-0200 and W911NF-23-1-0113). The authors acknowledged the facilities, and the scientific and technical assistance provided by the UNSW node of the Australian National Fabrication Facility (ANFF), and the Heavy Ion Accelerators (HIA) nodes at the University of Melbourne. ANFF and HIA are supported by the Australian Government through the National Collaborative Research Infrastructure Strategy (NCRIS) program. The authors acknowledged support from the Surface Analysis Laboratory, SSEAU, MWAC, UNSW for SIMS and the support of the International Atomic Energy Agency through the Cooperative Research Program number F11020 "Ion beam induced spatio-temporal structural evolution of materials: Accelerators for a new technology era". The authors thank Matthias Posselt for providing a modified version of his Crystal-TRIM code that was used to support ion implantation simulations. B.W. and X.Y. acknowledged support from the Sydney Quantum Academy. The views and conclusions contained in this document are those of the authors and should not be interpreted as representing the official policies, either expressed or implied, of the Army Research Office or the U.S. Government. The U.S. Government is authorized to reproduce and distribute reprints for Government purposes notwithstanding any copyright notation herein.

Open access publishing facilitated by University of New South Wales, as part of the Wiley - University of New South Wales agreement via the Council of Australian University Librarians.

Conflict of Interest

The authors declare no conflict of interest.

Data Availability Statement

The data that support the findings of this study are available from the corresponding author upon reasonable request.

Keywords

donors in silicon, ion implantation, molecule ions, quantum computing spin qubits

Received: September 27, 2023
Revised: December 7, 2023
Published online: January 12, 2024

[1] A. Chatterjee, P. Stevenson, S. De Franceschi, A. Morello, N. P. de Leon, F. Kuemmeth, *Nat. Rev. Phys.* **2021**, *3*, 157.
[2] G. Burkard, T. D. Ladd, A. Pan, J. M. Nichol, J. R. Petta, *Rev. Mod. Phys.* **2023**, *95*, 025003.
[3] M. T. Mądzik, S. Asaad, A. Youssry, B. Joecker, K. M. Rudinger, E. Nielsen, K. C. Young, T. J. Proctor, A. D. Baczewski, A. Laucht, V. Schmitt, F. E. Hudson, K. M. Itoh, A. M. Jakob, B. C. Johnson, D. N. Jamieson, A. S. Dzurak, C. Ferrie, R. Blume-Kohout, A. Morello, *Nature* **2022**, *601*, 348.
[4] A. Noiri, K. Takeda, T. Nakajima, T. Kobayashi, A. Sammak, G. Scappucci, S. Tarucha, *Nature* **2022**, *601*, 338.
[5] X. Xue, M. Russ, N. Samkharadze, B. Undseth, A. Sammak, G. Scappucci, L. M. Vandersypen, *Nature* **2022**, *601*, 343.
[6] A. R. Mills, C. R. Guinn, M. J. Gullans, A. J. Sigillito, M. M. Feldman, E. Nielsen, J. R. Petta, *Sci. Adv.* **2022**, *8*, eabn5130.
[7] B. E. Kane, *Nature* **1998**, *393*, 133.
[8] J. J. Pla, K. Y. Tan, J. P. Dehollain, W. H. Lim, J. J. Morton, D. N. Jamieson, A. S. Dzurak, A. Morello, *Nature* **2012**, *489*, 541.
[9] J. J. Pla, K. Y. Tan, J. P. Dehollain, W. H. Lim, J. J. Morton, F. A. Zwanenburg, D. N. Jamieson, A. S. Dzurak, A. Morello, *Nature* **2013**, *496*, 334.
[10] K. M. Itoh, H. Watanabe, *MRS Commun.* **2014**, *4*, 143.
[11] A. M. Tyryshkin, S. Tojo, J. J. Morton, H. Riemann, N. V. Abrosimov, P. Becker, H.-J. Pohl, T. Schenkel, M. L. Thewalt, K. M. Itoh, S. A. Lyon, *Nat. Mater.* **2012**, *11*, 143.
[12] K. Saeedi, S. Simmons, J. Z. Salvail, P. Dluhy, H. Riemann, N. V. Abrosimov, P. Becker, H.-J. Pohl, J. J. Morton, M. L. Thewalt, *Science* **2013**, *342*, 830.
[13] J. T. Muhonen, J. P. Dehollain, A. Laucht, F. E. Hudson, R. Kalra, T. Sekiguchi, K. M. Itoh, D. N. Jamieson, J. C. McCallum, A. S. Dzurak, A. Morello, *Nat. Nanotechnol.* **2014**, *9*, 986.
[14] P. Stano, D. Loss, *Nat. Rev. Phys.* **2022**, *4*, 672.
[15] M. Fuechsle, J. A. Miwa, S. Mahapatra, H. Ryu, S. Lee, O. Warschkow, L. C. Hollenberg, G. Klimeck, M. Y. Simmons, *Nat. Nanotechnol.* **2012**, *7*, 242.
[16] J. Wyrick, X. Wang, P. Namboodiri, R. V. Kashid, F. Fei, J. Fox, R. Silver, *ACS Nano* **2022**, *16*, 19114.
[17] L. Kranz, S. K. Gorman, B. Thorgrimsson, Y. He, D. Keith, J. G. Keizer, M. Y. Simmons, *Adv. Mater.* **2020**, *32*, 2003361.
[18] H. Büch, S. Mahapatra, M. Simmons, *Nat. Commun.* **2013**, *4*, 2017.
[19] J. Poate, K. Saadatmand, *Rev. Sci. Instrum.* **2002**, *73*, 868.
[20] J. Van Donkelaar, C. Yang, A. Alves, J. McCallum, C. Hougaard, B. Johnson, F. Hudson, A. Dzurak, A. Morello, D. Spemann, D. N. Jamieson, *J. Phys.: Condens. Matter* **2015**, *27*, 154204.
[21] D. N. Jamieson, W. I. Lawrie, S. G. Robson, A. M. Jakob, B. C. Johnson, J. C. McCallum, *Mater. Sci. Semicond. Process.* **2017**, *62*, 23.
[22] A. M. Jakob, S. G. Robson, V. Schmitt, V. Mourik, M. Posselt, D. Spemann, B. C. Johnson, H. R. Firgau, E. Mayes, J. C. McCallum, A. Morello, D. N. Jamieson, *Adv. Mater.* **2022**, *34*, 2103235.
[23] A. Morello, J. J. Pla, P. Bertet, D. N. Jamieson, *Adv. Quantum Technol.* **2020**, *3*, 2000005.
[24] R. Kalra, A. Laucht, C. D. Hill, A. Morello, *Phys. Rev. X* **2014**, *4*, 021044.
[25] M. T. Mądzik, A. Laucht, F. E. Hudson, A. M. Jakob, B. C. Johnson, D. N. Jamieson, K. M. Itoh, A. S. Dzurak, A. Morello, *Nat. Commun.* **2021**, *12*, 181.
[26] G. Tosi, F. A. Mohiyaddin, V. Schmitt, S. Tenberg, R. Rahman, G. Klimeck, A. Morello, *Nat. Commun.* **2017**, *8*, 450.
[27] F. A. Mohiyaddin, R. Rahman, R. Kalra, G. Klimeck, L. C. Hollenberg, J. J. Pla, A. S. Dzurak, A. Morello, *Nano Lett.* **2013**, *13*, 1903.
[28] R. Wilson, *J. Appl. Phys.* **1983**, *54*, 6879.
[29] J. W. Mayer, L. Eriksson, J. A. Davies, *Ion Implantation in Semiconductors*, Academic Press, New York **1970**.

[30] D. Holmes, B. Johnson, C. Chua, B. Voisin, S. Kocsis, S. Rubanov, S. Robson, J. McCallum, D. McCamey, S. Rogge, D. N. Jamieson, *Phys. Rev. Mater.* **2021**, *5*, 014601.
[31] D. F. Downey, J. W. Chow, E. Ishida, K. S. Jones, *Appl. Phys. Lett.* **1998**, *73*, 1263.
[32] A. M. Jakob, S. G. Robson, H. R. Firgau, V. Mourik, V. Schmitt, D. Holmes, M. Posselt, E. L. Mayes, D. Spemann, A. Morello, D. N. Jamieson, *arXiv preprint arXiv:2309.09626* **2023**.
[33] J. Smith, A. Budi, M. Per, N. Vogt, D. Drumm, L. Hollenberg, J. Cole, S. Russo, *Sci. Rep.* **2017**, *7*, 6010.
[34] W. M. Witzel, M. S. Carroll, A. Morello, Ł. Cywiński, S. D. Sarma, *Phys. Rev. Lett.* **2010**, *105*, 187602.
[35] S.-P. Jeng, T.-P. Ma, R. Canteri, M. Anderle, G. Rubloff, *Appl. Phys. Lett.* **1992**, *61*, 1310.
[36] J. F. Ziegler, M. D. Ziegler, J. P. Biersack, *Nucl. Instrum. Methods Phys. Res. B* **2010**, *268*, 1818.
[37] M. Posselt, J. Biersack, *Nucl. Instrum. Methods Phys. Res. B* **1992**, *64*, 706.
[38] H. G. Stemp, S. Asaad, M. R. van Blankenstein, A. Vaartjes, M. A. Johnson, M. T. Mądzik, A. J. Heskes, H. R. Firgau, R. Y. Su, C. H. Yang, A. Laucht, C. I. Ostrove, K. M. Rudinger, K. Young, R. Blume-Kohout, F. E. Hudson, A. S. Dzurak, K. M. Itoh, A. M. Jakob, B. C. Johnson, D. N. Jamieson, A. Morello, *arXiv preprint arXiv:2309.15463* **2023**.
[39] B. Joecker, A. D. Baczewski, J. K. Gamble, J. J. Pla, A. Saraiva, A. Morello, *New J. Phys.* **2021**, *23*, 073007.
[40] T. Sedgwick, *J. Electrochem. Soc.* **1983**, *130*, 484.
[41] S. Saito, S. Shishiguchi, A. Mineji, T. Matsuda, *MRS Online Proc. Libr. (OPL)* **1998**, *532*, 3.
[42] G. Oehrlein, S. Cohen, T. Sedgwick, *Appl. Phys. Lett.* **1984**, *45*, 417.
[43] S. Ruffell, I. Mitchell, P. Simpson, *J. Appl. Phys.* **2005**, *97*, 12.
[44] N. Cowern, D. Godfrey, D. Sykes, *Appl. Phys. Lett.* **1986**, *49*, 1711.
[45] J. Christensen, H. H. Radamson, A. Y. Kuznetsov, B. Svensson, *Appl. Phys. Lett.* **2003**, *82*, 2254.
[46] A. Vanderpool, A. Budrevich, M. Taylor, in *AIP Conference Proceedings*, vol. *866*, American Institute of Physics, College Park **2006**, pp. 41–45.
[47] C. Szeles, B. Nielsen, P. Asoka-Kumar, K. G. Lynn, M. Anderle, T. Ma, G. Rubloff, *J. Appl. Phys.* **1994**, *76*, 3403.
[48] C. G. Van de Walle, F. McFeely, S. T. Pantelides, *MRS Online Proc. Libr. (OPL)* **1988**, *141*, https://doi.org/10.1557/PROC-141-425.
[49] Y. Ono, M. Tabe, Y. Sakakibara, *Appl. Phys. Lett.* **1993**, *62*, 375.
[50] G. Feher, *Phys. Rev.* **1959**, *114*, 1219.
[51] M. Steger, T. Sekiguchi, A. Yang, K. Saeedi, M. Hayden, M. Thewalt, K. M. Itoh, H. Riemann, N. Abrosimov, P. Becker, H.-J. Pohl, *J. Appl. Phys.* **2011**, *109*, 102411.
[52] J. L. Ivey, R. L. Mieher, *Phys. Rev. B* **1975**, *11*, 822.
[53] A. Morello, J. J. Pla, F. A. Zwanenburg, K. W. Chan, K. Y. Tan, H. Huebl, M. Möttönen, C. D. Nugroho, C. Yang, J. A. Van Donkelaar, A. D. C. Alves, D. N. Jamieson, C. C. Escott, L. C. L. Hollenberg, R. G. Clark, A. S. Dzurak, *Nature* **2010**, *467*, 687.
[54] A. Laucht, R. Kalra, J. T. Muhonen, J. P. Dehollain, F. A. Mohiyaddin, F. Hudson, J. C. McCallum, D. N. Jamieson, A. S. Dzurak, A. Morello, *Appl. Phys. Lett.* **2014**, *104*, 9.
[55] M. T. Mądzik, T. D. Ladd, F. E. Hudson, K. M. Itoh, A. M. Jakob, B. C. Johnson, J. C. McCallum, D. N. Jamieson, A. S. Dzurak, A. Laucht, A. Morello, *Sci. Adv.* **2020**, *6*, eaba3442.